IEEE Access
Multidisciplinary | Rapid Review | Open Access Journal

Received October 9, 2018, accepted October 21, 2018, date of publication October 26, 2018, date of current version November 30, 2018.

Digital Object Identifier 10.1109/ACCESS.2018.2878278

Modal Decoupled Dynamics-Velocity Feed-Forward Motion Control of Multi-DOF Robotic Spine Brace

XINJIAN NIU[1], CHIFU YANG[1], BOWEN TIAN[2], XIANG LI[1], JUNWEI HAN[1], AND SUNIL K. AGRAWAL[3], (Member, IEEE)

[1]State Key Laboratory of Robotics and System, Harbin Institute of Technology, Harbin 150001, China
[2]Department of Economic and Trade, School of Business Administration, Zhongnan University of Economics and Law, Wuhan 430000, China
[3]Robotics and Rehabilitation Laboratory, Department of Mechanical Engineering, Columbia University, New York, NY 10027, USA

Corresponding author: Xiang Li (lxiang0818@163.com)

This work was supported in part by the National Natural Science Foundation of China under Grant 51305095 and the Natural Science Foundation of Heilongjiang Province under Grant QC2013C045.

ABSTRACT Based on the parallel robotic manipulator, this paper proposes a motion control strategy for the novel robotic spine brace for spinal rehabilitation exercises. However, several shortcomings of this parallel robotic manipulator, such as dynamic coupling in joint space, low response frequency in roll and pitch directions, and bad influence of device's gravity, result in bad effects on the performance of the robotic spine brace system. For solving these problems of parallel robotic manipulator, a new motion control structure, modal space dynamics-velocity feed-forward (MSDF) motion control strategy, is designed in this paper. A robotic spine brace system model and an actuator dynamic model are expressed using the Kane method. Stability of the robotic system with the MSDF control method is analyzed. For evaluating the performances of the proposed motion control structure, an experimental parallel robotic manipulator is built. Experimental results reveal that the presented MSDF motion control strategy can eliminate those disadvantages efficiently.

INDEX TERMS Robotic spine brace, parallel robotic manipulator, modal space dynamics-velocity feed-forward (MSDF), system model, stability.

I. INTRODUCTION

Spine is the backbone of human body which has the function of bearing weight, shock absorption, protection and movement [1]. When the body is injured in the spine, it seriously affects daily activities and reduces the quality of life. Thus, it is necessary for patients with spinal injury to do spinal rehabilitation exercises every day [2]–[4]. The current spinal rehabilitation exercises are mainly done by spinal rehabilitative trainers [5], [6], which is expensive and inconvenient for patients.

Human spine has six degree-of-freedoms (DOFs) movements on three planes. Thus, for achieving better rehabilitative effects, spinal rehabilitation exercises must be exerted on six motion directions [7], [8]. This paper proposes a novel motion control structure for the robotic spine brace based on the parallel robotic manipulator system, which applies 6 DOFs spine rehabilitative exercises for patients [9]. This parallel mechanism has several advantages including high-accuracy, big power-to-weight ratio and high robust stability [10]–[12]. Nevertheless, this parallel structure has several shortcomings, dynamic coupling in joint space, low response frequency in roll and pitch directions and bad influence of device's gravity. These inherent properties greatly affect and limit the performance of robotic spine brace and it is difficult to eliminate bad effects just using the classical proportion integral derivative (PID) control strategy in joint space or task space [13], [14]. Parallel robotic manipulators have been widely studied in some literatures [15]–[18], and have been practically applied in many areas [19]–[21]. In order to solve these boring problems, many effective control strategies have been designed for parallel robotic manipulators [22]–[24]. Those control methods are all proposed in work space or joint space [25]–[28]. Pi and Wang [29] designed a cascade control algorithm with a disturbance observer for 6-DOF parallel hydraulic manipulator in joint space coordinate, without considering the complex dynamics and direct kinematics of the system. Chen and Fu [30] proposed a backstepping control strategy with an observer-based

2169-3536 © 2018 IEEE. Translations and content mining are permitted for academic research only.
Personal use is also permitted, but republication/redistribution requires IEEE permission.
See http://www.ieee.org/publications_standards/publications/rights/index.html for more information.

forward kinematics solver for the 6-DOF parallel manipulator (Stewart platform) considering the friction of the actuator. In order to solve these boring problems, Yang *et al.* [31] and Yang and Junwei [32] proposed a novel modal space decouple control strategy for motion trajectory tracking. This new control strategy based on the typical PID control method solved the coupling problem of the parallel mechanism, but the gravity of the parallel system was ignored. In this paper a new effective control structure is developed in motion area, which overcomes those disadvantages.

This paper designs a novel motion control strategy, MSDF motion control structure for the parallel mechanism. This control structure can solve those boring inherent properties including dynamic coupling in physical space, low response frequency in roll and pitch directions and device's gravity. Compared with those control frameworks in joint space and work space, the presented motion control method improves the performance of parallel robotic manipulator excellently.

II. SYSTEM MODEL

Two Stewart-Gough platforms connected in series forms the dynamic brace system. The system has twelve DOFs driven by twelve linear electric cylinders and each limb has the same kinematic chain of universal-prismatic-spherical (UPS) shown in Fig 1. This paper just analyses the kinematics and dynamics of the lower platform, which can be extended to another platform.

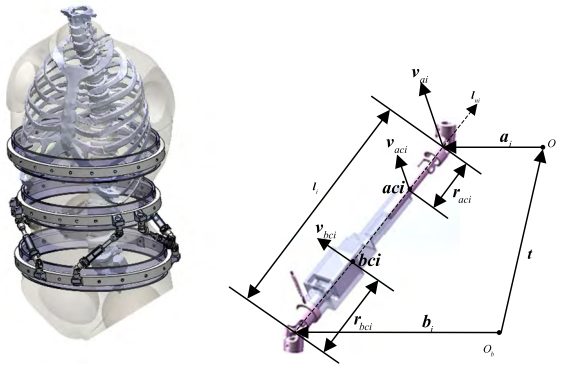

FIGURE 1. Geometry and parameterization of the new brace.

A. DYNAMICS MODEL

In order to establish the dynamic model of the parallel mechanism better, we make several assumptions including the upper and lower platforms, the cylinder and piston rod and the connectors are all rigid bodies and masses of the connectors are ignored. Based on those assumptions, the parallel robotic brace system comprises of thirteen rigid bodies which include one motion platform, six cylinders and six piston rods. According to the angular momentum theorem and the Newton's second law, inertia force and moment can be described

$$\boldsymbol{F}_p = \boldsymbol{m}_p \ddot{\boldsymbol{t}} \tag{1}$$

$$\boldsymbol{M}_p = \boldsymbol{I}_p \dot{\boldsymbol{\omega}}^L + \boldsymbol{\omega}^L \times \boldsymbol{I}_p \boldsymbol{\omega}^L \tag{2}$$

where $\boldsymbol{m}_p$ is the mass of the moving platform. $\boldsymbol{t}$ denotes the translation vector of the moving coordinate frame relative to the inertial coordinate frame. $\boldsymbol{\omega}^L$ means the angular velocity vector of the moving platform in the inertial coordinate frame. $\boldsymbol{I}_p$ is the inertia tensor in the fixed coordinate frame, which is regarded as

$$\boldsymbol{I}_p = \boldsymbol{R}\boldsymbol{I}_p^p\boldsymbol{R}^T \tag{3}$$

where $\boldsymbol{I}_p^p$ is the inertia tensor in the moving coordinate frame and $\boldsymbol{R}$ is the direction cosine matrix from the moving coordinate frame to the fixed coordinate frame.

Combine (1) with (2), generalized inertia force of platform can be described as

$$\begin{aligned}\boldsymbol{F}_p^* &= -\boldsymbol{M}_p\ddot{\boldsymbol{q}} - \boldsymbol{C}_p\dot{\boldsymbol{q}} \\ &= \begin{pmatrix} \boldsymbol{m}_p\boldsymbol{I} & 0 \\ 0 & \boldsymbol{I}_p \end{pmatrix} \begin{bmatrix} \ddot{\boldsymbol{t}} \\ \dot{\boldsymbol{\omega}}^L \end{bmatrix} - \begin{pmatrix} 0_{3\times3} & 0 \\ 0_{3\times3} & \tilde{\boldsymbol{\omega}}^L\boldsymbol{I}_p \end{pmatrix} \begin{bmatrix} \dot{\boldsymbol{t}} \\ \boldsymbol{\omega}^L \end{bmatrix}\end{aligned} \tag{4}$$

where $\tilde{\boldsymbol{\omega}}^L$ is the skew symmetric matrix of angular velocity vector in the fixed coordinate frame and $\dot{\boldsymbol{q}}$ is the generalized velocity in the fixed coordinate frame.

Similarly, using the Newton's second law and the angular momentum theorem, inertia force and inertia moment of piston rod can be written as

$$\boldsymbol{F}_{rvi} = \boldsymbol{m}_a \dot{\boldsymbol{v}}_{aci} \tag{5}$$

$$\boldsymbol{M}_{rwi} = \boldsymbol{I}_{ai}\dot{\boldsymbol{\omega}}_{li} + \boldsymbol{\omega}_{li} \times \boldsymbol{I}_{ai}\boldsymbol{\omega}_{li} \tag{6}$$

where $\boldsymbol{m}_a$ is the mass of piston rod. $\boldsymbol{v}_{aci}$ is the centroid velocity of piston rod. $\boldsymbol{\omega}_{li}$ is the angular velocity of leg. $\boldsymbol{I}_{ai}$ is the inertia tensor of piston rod.

The angular velocity of the leg and the centroid velocity of piston rod can be described using the generalized velocity of the moving platform

$$\boldsymbol{v}_{aci} = \boldsymbol{J}_{aci,ai}\boldsymbol{J}_{ai,q}\dot{\boldsymbol{q}} \tag{7}$$

$$\boldsymbol{\omega}_{li} = \boldsymbol{J}_{wi,ai}\boldsymbol{J}_{ai,q}\dot{\boldsymbol{q}} \tag{8}$$

$\boldsymbol{J}_{aci,ai}$ is the Jacobi matrix between the upper hinge point velocity and the centroid velocity of piston rod. $\boldsymbol{J}_{ai,q}$ is the Jacobi matrix between the generalized velocity of the moving platform and the upper hinge point velocity. $\boldsymbol{J}_{wi,ai}$ is the Jacobi matrix between the upper hinge point velocity and the angular velocity of the leg.

Combine (5), (6), and (7) with EQ (8), the generalized inertia force of piston rod in the inertial coordinate frame can be obtained

$$\begin{aligned}\boldsymbol{F}_{ri}^* &= \boldsymbol{J}_{ai,q}^T\boldsymbol{J}_{aci,ai}^T\boldsymbol{F}_{rvi} + \boldsymbol{J}_{ai,q}^T\boldsymbol{J}_{wi,ai}^T\boldsymbol{M}_{rwi} \\ &= \boldsymbol{J}_{ai,q}^T\left(\boldsymbol{J}_{aci,ai}^T\boldsymbol{m}_a\boldsymbol{J}_{aci,ai} + \boldsymbol{J}_{wi,ai}^T\boldsymbol{I}_{ai}\boldsymbol{J}_{wi,ai}\right)\boldsymbol{J}_{ai,q}\ddot{\boldsymbol{q}} + \\ &\quad \left\{\begin{array}{l} \boldsymbol{J}_{ai,q}^T\left[\boldsymbol{J}_{aci,ai}^T\boldsymbol{m}_a d\left(\boldsymbol{J}_{aci,ai}\boldsymbol{J}_{ai,q}\right)/dt\right] \\ +\boldsymbol{J}_{ai,\bar{q}}^T\boldsymbol{J}_{wi,ai}^T\left[\begin{array}{l}\boldsymbol{I}_{ai}d\left(\boldsymbol{J}_{wi,ai}\boldsymbol{J}_{ai,\bar{q}}\right)/dt \\ +\boldsymbol{J}_{wi,ai}\boldsymbol{J}_{ai,q}\dot{\bar{\boldsymbol{q}}} \times \boldsymbol{I}_{ai}\boldsymbol{J}_{wi,ai}\boldsymbol{J}_{ai,q}\end{array}\right] \end{array}\right\}\dot{\bar{\boldsymbol{q}}}\end{aligned} \tag{9}$$

(10)

where $\boldsymbol{m}_b$ is the mass of the cylinder. $\boldsymbol{I}_{bi}$ is the inertia tensor of the cylinder. $\boldsymbol{J}_{bci,ai}$ is the Jacobi matrix between upper hinge point velocity and centroid velocity of the cylinder.

Based on the Kane method and combine (4), (9) with (10), the dynamic model of the system can be expressed as

$$\boldsymbol{\tau} - \boldsymbol{F}_c + \boldsymbol{F}_p^* + \sum_{i=1}^{6} \boldsymbol{F}_{ri}^* + \sum_{i=1}^{6} \boldsymbol{F}_{ci}^* + \boldsymbol{G}^* = 0 \tag{11}$$

where $\boldsymbol{F}_c$ is the contact force. $\boldsymbol{G}^*$ is the gravity of system. $\boldsymbol{\tau}$ is the generalized force and can be written as

$$\boldsymbol{\tau} = \boldsymbol{J}_{lq}^T \boldsymbol{F}_a \tag{12}$$

where $\boldsymbol{J}_{lq}^T$ is the Jacobi matrix between the generalized velocity and the velocity of leg. $\boldsymbol{F}_a$ is the net actuator output force.

According to (11), the standard formula of multi rigid body dynamic model in task space can be rewritten as

$$\boldsymbol{M}(q)\ddot{\boldsymbol{q}} + \boldsymbol{N}(q, \dot{q})\dot{\boldsymbol{q}} + \boldsymbol{G}(q) + \boldsymbol{F}_c = \boldsymbol{\tau} \tag{13}$$

where $\boldsymbol{M}$ is mass matrix of system. $\boldsymbol{N}$ is the centrifugal term. $\boldsymbol{G}$ is the gravity term. q is the generalized pose of the moving platform.

Besides, in joint space, (13) can be rewritten as

$$\boldsymbol{M}_l(l)\ddot{\boldsymbol{l}} + \boldsymbol{C}_l(l, \dot{l})\dot{\boldsymbol{l}} + \boldsymbol{G}_l(l) + \boldsymbol{F}_{cl} = \boldsymbol{F}_a \tag{14}$$

where $\boldsymbol{M}_l$ is the mass matrix in joint space. $\boldsymbol{C}_l$ is the centrifugal force. $\boldsymbol{G}_l$ is the gravity term. The joint space and task space can be connected using the Jacobi matrix $\boldsymbol{J}_{lq}$.

$$\begin{aligned}
\dot{\boldsymbol{l}} &= \boldsymbol{J}_{lq}\dot{\boldsymbol{q}} \\
\boldsymbol{M}_l &= \boldsymbol{J}_{lq}^{-T}\boldsymbol{M}\boldsymbol{J}_{lq}^{-1} \\
\boldsymbol{C}_l &= \boldsymbol{J}_{lq}^{-T}\left(\boldsymbol{M}\dot{\boldsymbol{J}}_{lq}^{-1} + \boldsymbol{N}\boldsymbol{J}_{lq}^{-1}\right) \\
\boldsymbol{F}_{cl} &= \boldsymbol{J}_{lq}^{-T}\boldsymbol{F}_c \\
\boldsymbol{G}_l &= \boldsymbol{J}_{lq}^{-T}\boldsymbol{G}
\end{aligned}$$

The mass matrix of the robotic system in joint space is a real symmetric and positive definite matrix [33].

B. KINEMATICS MODEL

The kinematics of parallel robotic manipulators has been widely studied in [34]–[36]. Thus, the kinematics of the system is not described in detail in this section. As shown in Fig 1, using geometric method, the inverse kinematics can be expressed as

$$l_i = \sqrt{\boldsymbol{l}_i^T \boldsymbol{l}_i} = \sqrt{\left(\boldsymbol{t} + \boldsymbol{R}\boldsymbol{a}_i^p - \boldsymbol{b}_i\right)^T \left(\boldsymbol{t} + \boldsymbol{R}\boldsymbol{a}_i^p - \boldsymbol{b}_i\right)} \tag{15}$$

where l_i is the length of each actuator. $\boldsymbol{a}_i^p$ shows the radius vector of the upper joint point in the moving framework and $\boldsymbol{b}_i$ is the radius vector of the lower joint points in fixed framework.

The analysis of the forward kinematic is aimed at achieving the position of the upper platform using the given length of limb. In this paper, the Newton-Raphson iterative algorithm is used to achieve the position of the platform. The iterative sequence of this algorithm can be expressed as

$$q_{j+1} = q_j + \boldsymbol{J}_{lq}^{-1}(l_m - l_j) \tag{16}$$

where l_m is the measured actuator position.

C. ACTUATOR DYNAMICS

This parallel structure is driven by twelve electric cylinders. The force equilibrium equation is presented without considering the actuator's friction.

$$\boldsymbol{F}_p = \boldsymbol{F}_a \tag{17}$$

where $\boldsymbol{F}_p$ is the output force of the actuator. $\boldsymbol{F}_a$ can be measured using the force sensor.

According to the output force principle of motor and the manufacturer information, the output force of actuator $\boldsymbol{F}_p$ can be described as

$$\boldsymbol{F}_p = k_t \boldsymbol{I}_t \tag{18}$$

where k_t is the force coefficient of motor and $\boldsymbol{I}_t$ is the equivalent current deduced from one current loop which is equivalent to the first order inertia link and the expression is

$$\boldsymbol{I}_t = \frac{1}{\tau_0 s + 1}\boldsymbol{U} \tag{19}$$

where τ_0 is the time constant of the equivalent current loop. $\boldsymbol{U}$ is the input of the current loop and can be expressed as

$$U_i = U_{ri} - k_e \dot{l}_i \tag{20}$$

where k_e is the equivalent electromotive force (EMF) coefficient and U_{ri} is the control voltage of the ith motor.

III. CONTROL DESIGN

A. PID MOTION CONTROL STRATEGY IN TRADITIONAL PHYSICAL SPACE

Traditional physical space can be divided into two control space, joint space and task space. Because of measuring poses of end effector with difficulty, the joint space control strategy (JSCS) is applied in practice extensively. Thus, only the JSCS is presented in this paper as an active force control strategy in traditional physical space shown in Fig 2.

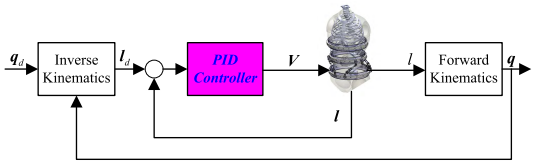

FIGURE 2. PID control strategy of motion simulator in traditional physical space.

In Fig 2, $\boldsymbol{q}_d$ is the desired generalized pose of motion simulator. $\boldsymbol{l}_d$ is the desired leg's position of motion simulator. Since the classical PID control scheme is widely used in practice, a typical P control method is adopted as the controller.

$$\boldsymbol{V} = k_p \boldsymbol{e} = k_p(\boldsymbol{l}_d - \boldsymbol{l}) \tag{21}$$

where k_p is the P control parameter which is tuned in the process of experiment.

B. PID CONTROL STRATEGY IN MODAL SPACE

In physical space, since the strong dynamic coupling of parallel structure, it is difficult to control MIMO robotic brace system. In this paper, modal space decouple method is applied to solve the dynamic coupling problem and improve performances of the robotic brace system. In modal space, parameters of each channel can be tuned independently [37]. Fig 3 shows the PID control structure of motion simulator in modal space.

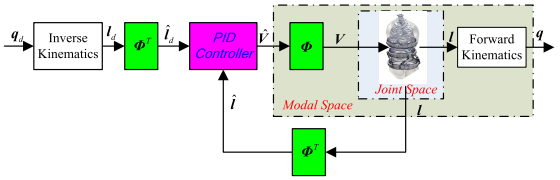

FIGURE 3. PID control strategy of motion simulator in modal space.

In Fig 3, $\boldsymbol{\Phi}$ is modal matrix. $\hat{\boldsymbol{l}}_d$ is the desired leg's position in modal space. $\hat{\boldsymbol{l}}$ is the actual leg's position in modal space. $\hat{\boldsymbol{V}}$ is the input voltage in modal space. In traditional joint space, $\boldsymbol{V}$ is input of the parallel robotic manipulator. In modal space, the dynamic system is controlled using modal space decoupling strategy. The output of the controller is $\hat{\boldsymbol{V}}$ and $\hat{\boldsymbol{l}}$ is the feedback position of the leg in modal space.

In modal space, each channel is controlled independently [37]. To reveal this property, the classical P control strategy is also employed as the control law

$$\hat{\boldsymbol{V}} = \hat{\boldsymbol{K}}_p\hat{\boldsymbol{e}} = \begin{bmatrix} \hat{k}_1 & & & \\ & \hat{k}_2 & & \\ & & \ddots & \\ & & & \hat{k}_6 \end{bmatrix} \begin{bmatrix} \hat{l}_{d1} - \hat{l}_1 \\ \hat{l}_{d2} - \hat{l}_2 \\ \vdots \\ \hat{l}_{d6} - \hat{l}_6 \end{bmatrix} \tag{22}$$

where $\hat{k}_i$ is the *ith* P control parameter in modal space. $\hat{\boldsymbol{e}}$ is the control error in modal space, $\hat{\boldsymbol{e}} = \hat{\boldsymbol{l}}_d - \hat{\boldsymbol{l}}$.

C. DYNAMICS-VELOCITY FEED-FORWARD CONTROL STRATEGY IN MODAL SPACE

In joint space and task space, since the strong dynamic coupling of parallel robotic manipulator, it is impossible to control MIMO dynamic system independently. In order to decouple the dynamic coupling system and improve the system performance, the modal space decoupling technique is used in this paper. In modal space, parameters of each channel can be tuned independently [37]. As shown in Fig 4, the MIMO system is controlled in modal space where each channel is controlled independently.

In Fig 4, k_v is the velocity feed forward gain. k_F is the dynamic feed forward gain.

Based on the feed-forward method, we design the modal space control law without affecting the stability of the modal space PID (MSPID) system.

$$\hat{\boldsymbol{V}} = k_v\dot{\hat{\boldsymbol{l}}}^d + k_F\hat{\boldsymbol{F}}_{Ld} \tag{23}$$

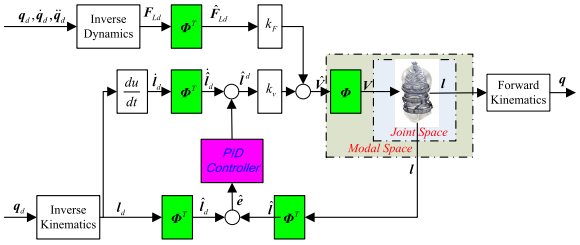

FIGURE 4. MSDF control strategy of motion simulator.

$$\hat{\boldsymbol{l}}^d = \dot{\hat{\boldsymbol{l}}}_d + \hat{\boldsymbol{K}}_p\hat{\boldsymbol{e}} = \dot{\hat{\boldsymbol{l}}}_d + \hat{\boldsymbol{K}}_p\left(\hat{\boldsymbol{l}}_d - \hat{\boldsymbol{l}}\right) \tag{24}$$

$$\hat{\boldsymbol{F}}_{Ld} = \boldsymbol{\Phi}^T\left(\boldsymbol{G}_{ld} + \boldsymbol{M}_{ld}\ddot{\boldsymbol{l}}_d\right) \tag{25}$$

where $\boldsymbol{M}_{ld}$ is the mass matrix in desired poses. $\boldsymbol{G}_{ld}$ is the gravity term in desired poses
(25) can be rewritten as

$$\hat{\boldsymbol{F}}_{Ld} = \hat{\boldsymbol{G}}_{ld} + \hat{\boldsymbol{M}}_{ld}\ddot{\hat{\boldsymbol{l}}}_d \tag{26}$$

where $\hat{\boldsymbol{M}}_{ld}$ is the desired modal mass matrix, $\hat{\boldsymbol{M}}_{ld} = diag\left\{\hat{M}_{ld1} \ \cdots \ \hat{M}_{ld6}\right\}$. $\hat{\boldsymbol{G}}_{ld}$ is the desired modal gravity term, $\hat{\boldsymbol{G}}_{ld} = \left[\hat{G}_{ld1} \ \cdots \ \hat{G}_{ld6}\right]$.

Base on Laplace transformation, (23), (24) and (26) can be expressed as

$$\hat{\boldsymbol{V}} = k_v\hat{\boldsymbol{l}}^d(s) + k_F\hat{\boldsymbol{F}}_{Ld}(s) \tag{27}$$

$$\hat{\boldsymbol{l}}^d = \hat{\boldsymbol{K}}_p\left[\left(s\hat{\boldsymbol{K}}_p^{-1} + \boldsymbol{I}_{6\times6}\right)\hat{\boldsymbol{l}}_d - \hat{\boldsymbol{l}}\right] \tag{28}$$

$$\hat{\boldsymbol{F}}_{Ld} = \hat{\boldsymbol{G}}_{ld} + s^2\hat{\boldsymbol{M}}_{ld}\hat{\boldsymbol{l}}_d \tag{29}$$

Substitute (28) and (29) into (27), the modal space control law can be obtained

$$\hat{\boldsymbol{V}}(s) = k_v\hat{\boldsymbol{K}}_p\left[\left(\frac{k_F}{k_v}\hat{\boldsymbol{K}}_p^{-1}\hat{\boldsymbol{M}}_{ld}s^2 + \hat{\boldsymbol{K}}_p^{-1}s + \boldsymbol{I}_{6\times6}\right)\hat{\boldsymbol{l}}_d - \hat{\boldsymbol{l}}\right] + k_F\hat{\boldsymbol{G}}_{ld} \tag{30}$$

(30) can be rewritten as

$$\hat{V}_i(s) = k_v\hat{k}_{pi}\left[\left(\frac{k_F\hat{M}_{ldi}}{k_v\hat{k}_{pi}}s + \frac{1}{\hat{k}_{pi}}s + 1\right)\hat{l}_{di} - \hat{l}_i\right] + k_F\hat{G}_{li} \tag{31}$$

It can be seen from (31) that the MSDF control law is equivalent to designing a two-order differential position feed-forward link and a gravity compensation term in each channel independently based on the MSPID control theory, as shown in Fig 5.

In Fig 5, the feed-forward loop can be expressed as

$$G_D(s) = diag(G_{D1}(s) \ \cdots \ G_{D6}(s)) \tag{32}$$

$$G_{Di}(s) = \frac{k_F\hat{M}_{ldi}}{k_v\hat{k}_{pi}}s + \frac{1}{\hat{k}_{pi}}s + 1, \quad i = 1, 2, 3\ldots, 6 \tag{33}$$

In each channel, the control parameters of the MSDF control method can be tuned independently. Based on the property of each channel, the designed controller makes each modal channel reach to optimal performances. Therefore, the best performances of the parallel mechanism system can be achieved.

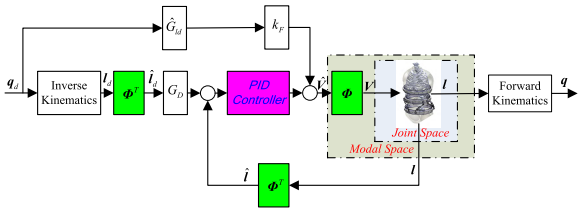

FIGURE 5. Equivalent MSDF control strategy of motion simulator.

IV. STABILITY ANALYSIS

Stability is the most important performance of the parallel robotic manipulator system. Since the dynamic feed-forward control method has no damage to the stability of the whole system, this paper analyzes the stability of the MSPID system.

Combine (18), (19) with (20), we can get

$$k_t^{'}(\boldsymbol{U}_r - k_e\dot{l}) = \boldsymbol{F}_p \tag{34}$$

where $k_t^{'} = k_t \frac{1}{\tau_0 s+1}$

After Laplace transformation, (35) can be expressed as

$$\boldsymbol{U}_r = k_e l s + \frac{1}{k_t^{'}}\boldsymbol{F}_p \tag{35}$$

Combine (14) with (17), (36) can be achieved

$$\boldsymbol{M}_l(l)\ddot{l} + \boldsymbol{C}_l(l,\dot{l})\dot{l} + \boldsymbol{G}_l(l) = \boldsymbol{F}_p \tag{36}$$

Since parallel robotic manipulator used for spine rehabilitation always works on low speed area, the contribution of centrifugal term $\boldsymbol{C}_l$ in corrective system is very small [37]. The influence of gravity on the steady-state accuracy of motion simulator system can be reduced by reasonable gravity compensation. Without loss of generality, (36) can be rewritten as

$$\boldsymbol{M}_l(l)\ddot{l} = \boldsymbol{F}_p \tag{37}$$

After Laplace transformation, (38) can be achieved

$$s^2 M_l(l) l = F_p \tag{38}$$

Substitute (35) into (38)

$$k_t \boldsymbol{U}_r = ls\left(\boldsymbol{M}_l\tau_0 s^2 + \boldsymbol{M}_l s + k_t k_e \boldsymbol{I}_{6\times 6}\right) \tag{39}$$

According to the relationship between the modal space and the joint space, we can get

$$\boldsymbol{M}_l = \boldsymbol{\Phi}\hat{\boldsymbol{M}}_l\boldsymbol{\Phi}^T \tag{40}$$

Substitute (40) into (39)

$$k_t \boldsymbol{U}_r = \boldsymbol{\Phi}\left(\hat{\boldsymbol{M}}_l\tau_0 s^2 + \hat{\boldsymbol{M}}_l s + k_t k_e \boldsymbol{I}_{6\times 6}\right)\boldsymbol{\Phi}^T \boldsymbol{l} s \tag{41}$$

Define

$$\hat{\boldsymbol{U}}_r = \boldsymbol{\Phi}^T\boldsymbol{U}_r, \quad \hat{\boldsymbol{l}} = \boldsymbol{\Phi}^T\boldsymbol{l} \tag{42}$$

where $\hat{\boldsymbol{U}}_r$ is the motor voltage in modal space.

Combine (41) with (42), (41) can be expressed as

$$k_t\hat{\boldsymbol{U}}_r = \hat{\boldsymbol{l}}s\left(\hat{\boldsymbol{M}}_l\tau_0 s^2 + \hat{\boldsymbol{M}}_l s + k_t k_e \boldsymbol{I}_{6\times 6}\right) \tag{43}$$

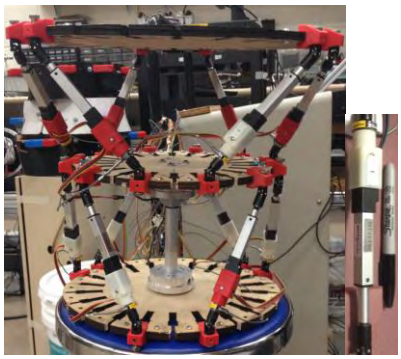

FIGURE 6. Experimental robotic brace.

Combine (17) with (43), the transfer function from $\hat{\boldsymbol{U}}_r$ to $\hat{\boldsymbol{l}}$ is achieved

$$\frac{k_t}{s\left(\hat{M}_{li}\tau_0 s^2 + \hat{M}_{li}s + k_t k_e\right)}\hat{U}_{ri} = \hat{l} \tag{44}$$

Since $\hat{U}_{ri} = \hat{V}_i$ EQ (44) can be rewritten as

$$\frac{k_t}{s\left(\hat{M}_{li}\tau_0 s^2 + \hat{M}_{li}s + k_t k_e\right)}\hat{V}_i = \hat{l} \tag{45}$$

Combine (22) with (45), the open loop transfer function of MSPID system is expressed as

$$\hat{G}_i(s) = \frac{\hat{l}_i}{\hat{l}_{di}} = \frac{\hat{k}_{pi}/k_e}{s\left(\frac{s^2}{k_t k_e/\tau_0\hat{M}_{li}} + \frac{2\hat{\xi}_i s}{\sqrt{k_t k_e/\tau_0\hat{M}_{li}}} + 1\right)} \tag{46}$$

where $\hat{\xi}_i$ is the damping coefficient, $\hat{\xi}_i = \frac{1}{2\sqrt{k_t k_e \tau_0/\hat{M}_{li}}}$. (46) can be written as

$$\hat{G}_i(s) = \frac{\hat{k}_{pi}/k_e}{s\left(\frac{s^2}{\hat{\omega}_{ni}^2} + \frac{2\xi_i s}{\hat{\omega}_{ni}} + 1\right)} \tag{47}$$

where $\hat{\omega}_{ni}$ is the natural frequency of the system, $\hat{\omega}_{ni} = \sqrt{k_t k_e/\tau_0\hat{M}_{li}}$.

According to stability criterion of logarithmic frequency characteristics, in order to guarantee the stability of the MSPID system, parameters of the system must satisfy (46).

$$\hat{k}_{pi}\hat{M}_{li}/k_e < 2\hat{\xi}_i\hat{\omega}_{ni} \tag{48}$$

It can be seen from (48) that by choosing appropriate control modal gain matrix $\hat{\boldsymbol{K}}_p$, the stability of the MSPID system is guaranteed. Therefore, the MSDF motion control system is guaranteed robustly stable.

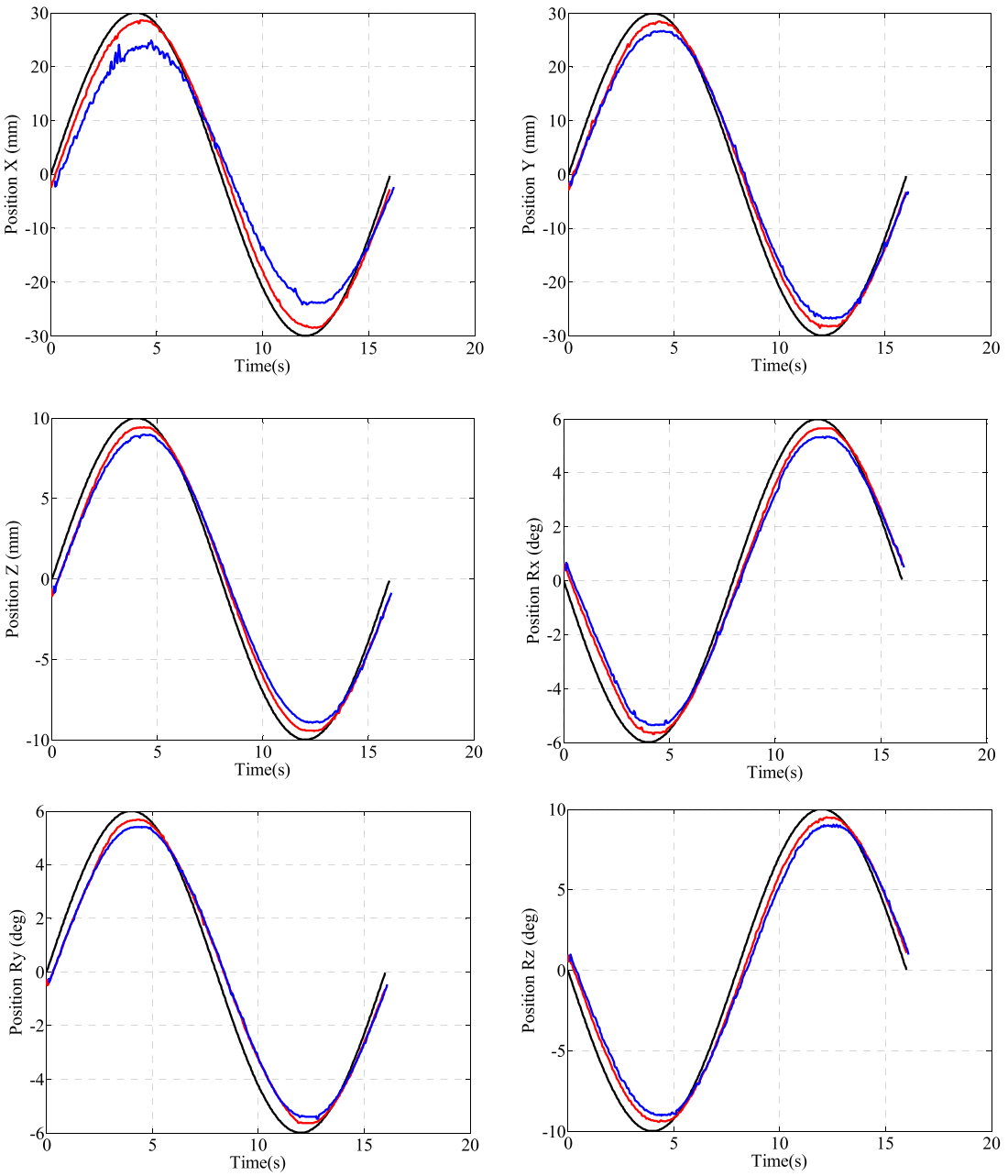

FIGURE 7. Responses to the desired sine signals in joint space; the black lines are the desired signals; the red lines are the responses with $k_p = diag$ (20 20 20 20 20 20), and the blue lines are the responses with $k_p = diag$ (4 20 20 20 20 20).

TABLE 1. Parameters of the experimental parallel robotic manipulator.

Parameters	Values
Ellipse's long distance of upper joint (mm)	150
Ellipse's short distance of upper joint (mm)	142
Ellipse's long distance of lower joint (mm)	170
Ellipse's long distance of lower joint (mm)	149
Max. stroke of linear actuator (mm)	50
Initial length of actuator (mm)	160
Mass of upper platform and joint (Kg)	0.33

V. EXPERIMENT

This section evaluates control performance based on MSDF control theory via experiment. In contrast to MSPID control method, MSDF control theory has better tracking performance.

A. EXPERIMENT SETUP

To implement and evaluate the performance of the proposed MSDF motion control strategy, an experimental parallel robotic manipulator is built in Fig 6, which has the following features: 1) twelve Firgelli miniature linear actuators, 2) a ATI 6-axis force sensor, 3) a NI-sbRIO real-time controller, 4) a monitor computer. The monitor computer provides the position reference signals and the motion controller is running in sbRIO. Table 1 shows geometric parameters of the intelligent system and the brace system sampling time is set to 20ms.

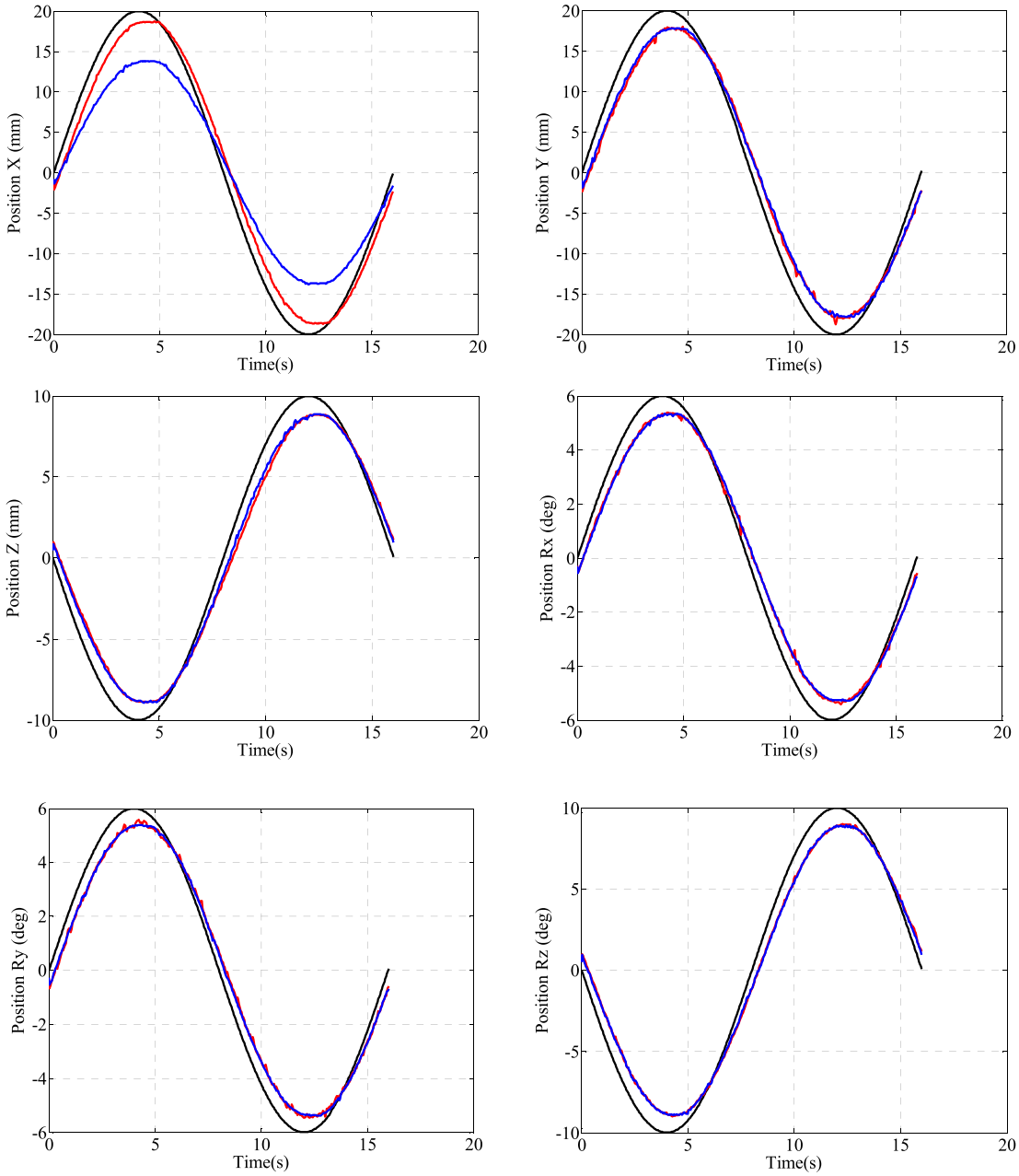

FIGURE 8. Responses to the desired sine signals in modal space; the black lines are the desired signals; the red lines are the responses with $\hat{k}_P = diag$ (20 20 20 20 20 20), and the blue lines are the responses with $\hat{k}_P = diag$ (4 20 20 20 20 20).

B. EXPERIMENT RESULTS

For clearly revealing strong dynamic coupling of the robotic system in joint space, the classical P control strategy is applied for the JSCS. The control parameter $k_p = diag\left(k_{p1}\ k_{p2}\ \cdots\ k_{p6}\right)$ is well tuned experimentally, $k_{pi} = 20.k_{pi}$ is the ith channel of the system. As shown in Fig 7, the desired sine signals, 30mm/0.06Hz in surge and sway, 10mm/0.06Hz in heave, 6deg/0.06Hz in roll and pitch and 10deg/0.08Hz in yaw are exerted on the robotic spine brace with the classical P control method. k_{pi} is changed to be 4 in turn. The responses to the reference signals are also shown in Fig 7 with the $k_p = diag(4\ \ 20\ \ 20\ \ 20\ \ 20\ \ 20)$.

Fig 7 shows that the change of the parameterk_{p1}affects not only the performance of X channel but performances of other channels. Similarly, the change of other parameters also affects the performance of all channels. That is to say, the change of any channel parameter will affect the performance of all channels in joint space. Thus, it is impossible to adjust each channel control parameter independently and the performance of each DOF is restricted by the properties of all channels.

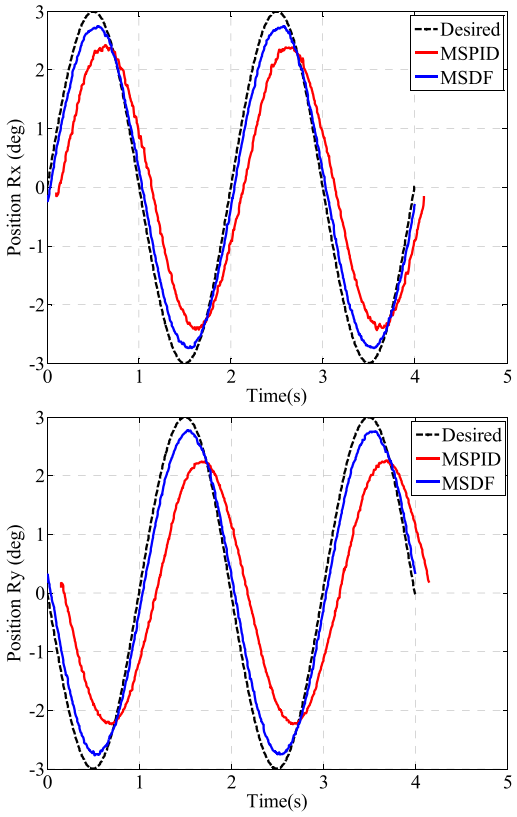

FIGURE 9. Responses to the desired sine signals with MSPID and MSDF controllers in roll and pitch directions.

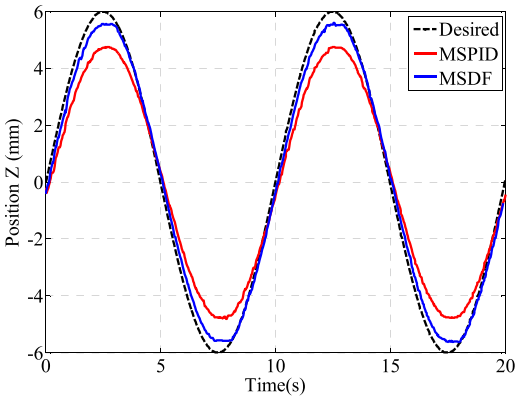

FIGURE 10. Responses to the desired sine signal with MSPID and MSDF controllers in heave direction.

For solving the boring dynamic coupling problem in joint space, this paper presents a modal space control strategy. In modal space, each channel parameter can be adjusted independently without affecting performances of other DOFs. As shown in Fig 8, the desired sine signals, 20mm/0.06Hz in surge and sway, 10mm/0.06Hz in heave, 6deg/0.06Hz in roll and pitch and 10deg/0.06Hz in yaw, are exerted on the robotic spine brace with the classical P control method. The responses with the parameters $\hat{k}_p = diag\,(20\ \ 20\ \ 20\ \ 20\ \ 20\ \ 20)$ and $\hat{k}_p = diag\,(4\ \ 20\ \ 20\ \ 20\ \ 20\ \ 20)$ are also shown in Fig 8.

It can be seen from Fig 8 that the change of X channel parameter in modal space just affects the performance of the first DOF. That is to say, the first channel controller can be designed independently without affecting performances of other DOFs. Similarly, other channel control parameters can also be tuned independently. Thus, the MSPID control method presented in this paper solves the strong dynamic coupling problem of the robotic spine brace in joint space.

Since other inherent properties of the parallel manipulator, such as low response frequency and bad influence of device's gravity, it is necessary to design novel control strategy to solve those problems. In order to achieve better performances, this paper proposes an MSDF control structure for the robotic manipulator. For verifying the performance of the system with this presented control method, several desired signals are given to the robotic system. The modal space P controllers are tuned to be

$$\hat{\boldsymbol{K}}_p = diag\,[20\ \ 20\ \ 20\ \ 20\ \ 20\ \ 20] \tag{49}$$

The dynamics-velocity feed-forward control parameters k_v and k_F are tuned to be

$$\begin{aligned} k_v &= diag\,[4.0\ \ 4.0\ \ 4.0\ \ 4.0\ \ 4.0\ \ 4.0] \\ k_F &= diag\,[1.6\ \ 1.6\ \ 1.6\ \ 1.6\ \ 1.6\ \ 1.6] \end{aligned} \tag{50}$$

In order to evaluate the low response frequency in roll and pitch directions, the desired sine signals 3deg/0.5Hz in roll and pitch are exerted on the robotic spine brace with the classical P control method. According to Fig 9, when the given signal frequency reaches 0.5Hz the lag of phase is 24° in roll and 33° in pitch and the attenuation of amplitude 21% in roll and 25% in pitch using the MSPID control strategy. However, the lag of phase is 6° in roll and 7° in pitch and the attenuation of amplitude is 9% in roll and 8% in pitch using the MSPID control strategy. Thus, the proposed MSDF control method can improve the response frequency excellently.

The gravity of the device mainly infects the performance in heave direction. In order to clearly reveal effects of the device gravity, the desired sine signals 6mm/0.1Hz in roll and pitch is exerted on the robotic spine brace with the classical P control method. Fig 10 shows that the attenuation of amplitude is 21% with MSPID control strategy while the attenuation of amplitude is 8% with the MSDF control method. Therefore, the designed MSDF control strategy can compensate the gravity of the device.

As shown in Fig 11, sine signals, 20mm/0.06Hz in surge and sway, 10mm/0.06Hz in heave, 6deg/0.06Hz in roll and pitch and 10deg/0.06Hz in yaw, are given to the robotic system in all six directions to detect the performance of the system. Compared with the MSPID control strategy, the attenuation of amplitude is a 65% decrease at least and the lag of phase is a 59% at least with the MSDF control method. Therefore, when the desired sine signals are applied on the robotic brace using the proposed MSDF control method,

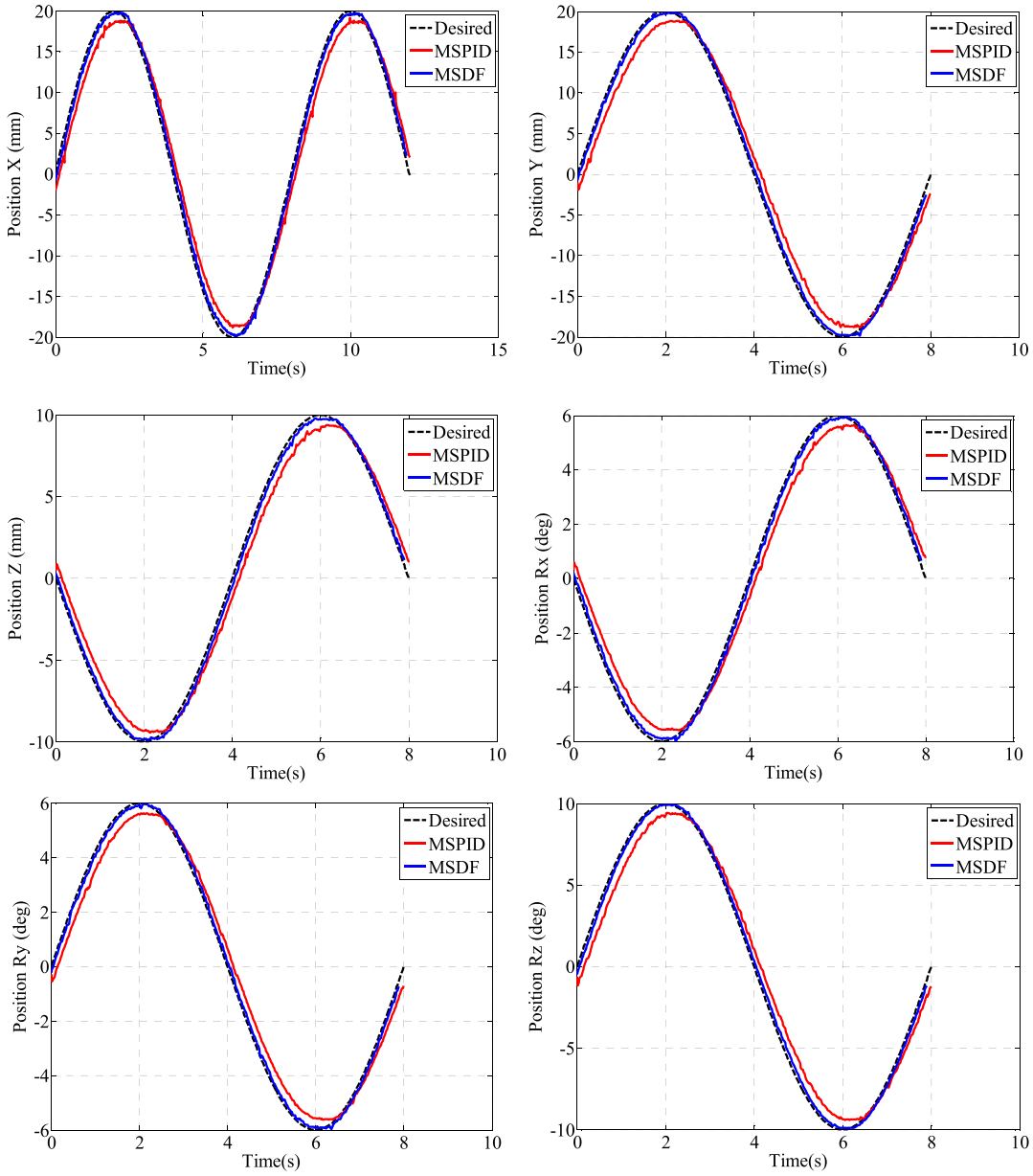

FIGURE 11. Responses to the desired sine signals with MSPID and MSDF controllers.

the intelligent robotic system can respond to the given signals than that of the MSPID control strategy.

The desired special motion signals are applied on the parallel manipulator in (51), respectively. Fig 12 shows the responses to the given special signals.

$$X = 5.8\sin(0.230t) + 9.0\sin(0.314t) + 8.3\sin(0.400t) \tag{51a}$$

$$Y = 7.6\sin(0.240t) + 4.1\sin(0.300t) + 9.9\sin(0.390t) \tag{51b}$$

$$Z = 6.2\sin(0.233t) + 7.2\sin(0.320t) + 3.9\sin(0.380t) \tag{51c}$$

$$R_x = 3.7\sin(0.240t) + 2.0\sin(0.310t) + 2.0\sin(0.377t) \tag{51d}$$

$$R_y = 4.0\sin(0.240t) + 1.5\sin(0.305t) + 3.0\sin(0.390t) \tag{51e}$$

$$R_z = 3.5\sin(0.300t) + 1.4\sin(0.314t) + 2.5\sin(0.400t) \tag{51f}$$

As can be seen from Fig 12, compared with the MSPID control strategy, the attenuation of amplitude is a 50% decrease at least and the lag of phase is a 56% at least with the MSDF control method. Thus, performances of the robotic spine brace with the MSDF control method are superior to that with the MSPID control strategy.

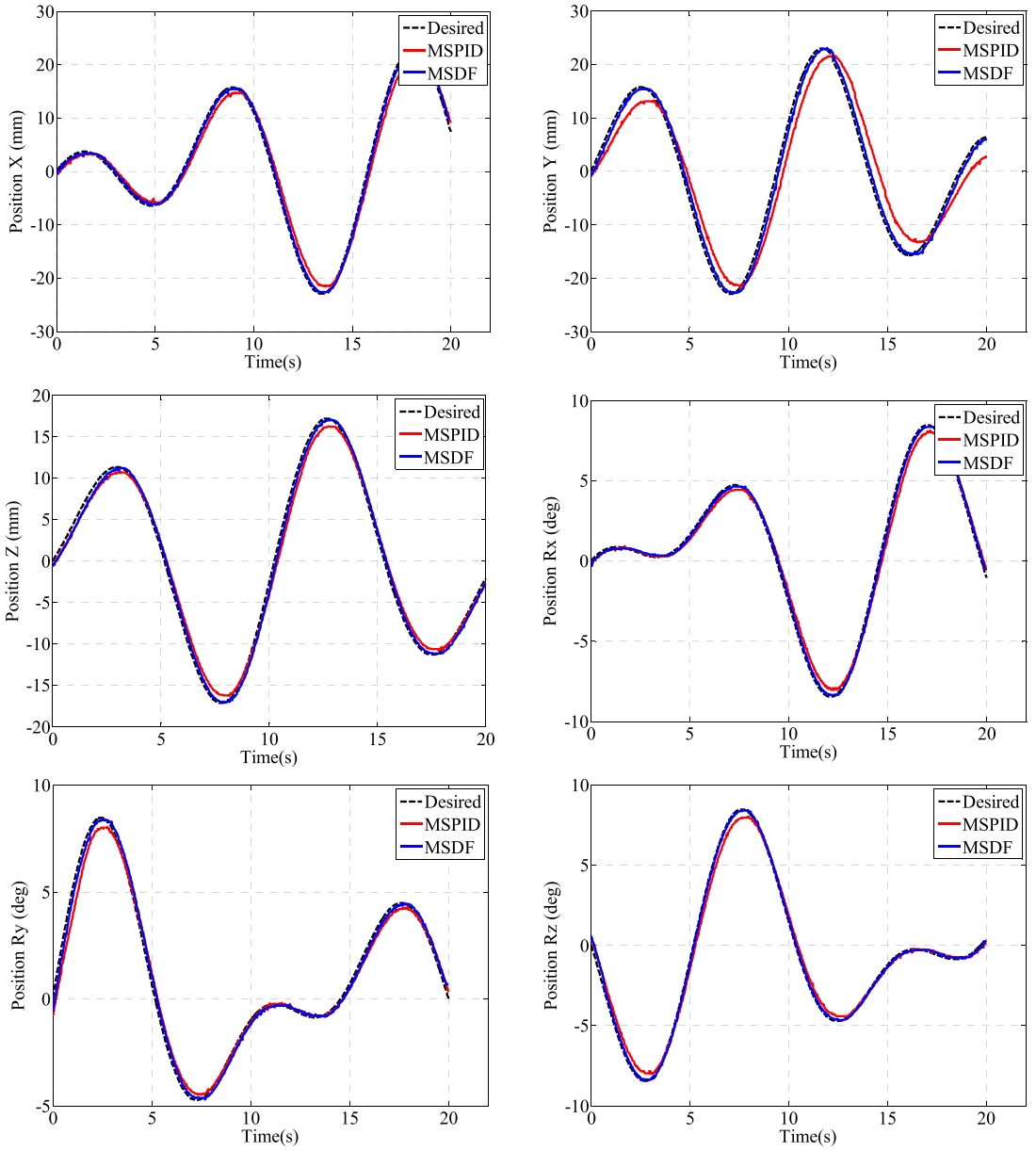

FIGURE 12. Responses to the special sine signals with MSPID and MSDF controllers.

It can be seen from Fig 7-Fig 12 that the proposed MSDF control strategy solves not only the dynamic coupling problem of the system but other boring problems. Thus, the MSDF motion control structure improves performances of the robotic spine brace remarkably. The novel control method tracks the desired dynamic trajectory more quickly and accurately, and offers six DOFs motions to adapt to the movement of the human's spine.

VI. CONCLUSION

This paper designs a MSDF control framework for parallel intelligent mechanism for overcoming those inherent problems. When using the classical motion control strategy, the inherent properties of parallel mechanism in joint space or work space greatly limit the performance of parallel robotic manipulator and result in big loss of positions in the direction and value. In order to capture negative effects of the system, the MSDF motion control structure is developed by combing the modal space decoupling theory with dynamic-velocity feed-forward control technique. Several experimental desired position signals are given to the robotic spine brace system to evaluate the performance of the parallel robotic manipulator with the novel MSDF control theory. It can be seen from experimental results that the MSDF control can track the desired dynamic motion trajectory more quickly and accurately, and exert high-precision motions in six directions on human spine.

The proposed MSDF motion control strategy is the novel control algorithm for the intelligent dynamic brace. Though the dynamic system can track the given dynamic motion signals excellently, there are several chances and challenges about the robotic brace system in the future. Currently, this intelligent robotic brace is a principle prototype which has not been applied on patients practically. Thus, more clinical trials are needed for verifying performances of the proposed control method in depth. The next step is exerting this robotic spine brace on patients using the novel control algorithm in practice. In this paper, the given signals are special motion signals. For rehabilitating patients' spine better, the real spinal trajectories should be adopted and applied on the human spine. Therefore, the electromyography (EMG) sensors will be used to detect the real daily motion trajectories of the human spine. Besides, the existence of uncertain disturbances, for example, frictions, modeling errors and the external environmental disturbances will damage the stability of the system. Thus, it is necessary to develop the MSDF control strategy based on and a disturbance observer in the future.

ACKNOWLEDGMENT

The authors would like to thank the editor, associate editor and reviewers for their constructive comments and suggestions to improve the quality of the paper.

REFERENCES

[1] I. R. A. Posner, A. A. White, III, W. T. Edwards, and W. C. Hayes, "A biomechanical analysis of the clinical stability of the lumbar and lumbosacral spine," *Spine*, vol. 7, no. 4, pp. 374–389, 1982.

[2] J. Rainville, C. Hartigan, E. Martinez, J. Limke, C. Jouve, and M. Finno, "Exercise as a treatment for chronic low back pain," *Spine J.*, vol. 4, no. 1, pp. 106–115, 2004.

[3] T. Kuru, İ. Yeldan, E. E. Dereli, A. R. Özdinçler, F. Dikici, and İ. Çolak, "The efficacy of three-dimensional Schroth exercises in adolescent idiopathic scoliosis: A randomised controlled clinical trial," *Clin. Rehabil.*, vol. 30, no. 2, pp. 181–190, 2016.

[4] S. Langensiepen *et al.*, "Home-based vibration assisted exercise as a new treatment option for scoliosis—A randomised controlled trial," *J. Musculoskeletal Neuronal Interact.*, vol. 17, no. 4, pp. 259–267, 2017.

[5] R. K. Hall and M. J. Rapport, "Physical therapy for a child with infantile idiopathic scoliosis and motor delay," *Pediatric Phys. Therapy*, vol. 29, no. 3, pp. E1–E6, 2017.

[6] K. I. M. Kewwan, D. Mullineaux, and J. E. O. N. Kyoungkyu, "Exercise rehabilitative approach to functional improvement in adult idiopathic scoliosis: A functional movement screen-based program," *Iranian J. Public Health*, vol. 47, no. 7, pp. 1041–1043, 2018.

[7] M.-J. Kim and D.-S. Park, "The effect of Schroth's three-dimensional exercises in combination with respiratory muscle exercise on Cobb's angle and pulmonary function in patients with idiopathic scoliosis," *Phys. Therapy Rehabil. Sci.*, vol. 6, no. 3, pp. 113–119, 2017.

[8] M. Monticone, E. Ambrosini, D. Cazzaniga, B. Rocca, and S. Ferrante, "Active self-correction and task-oriented exercises reduce spinal deformity and improve quality of life in subjects with mild adolescent idiopathic scoliosis. Results of a randomised controlled trial," *Eur. Spine J.*, vol. 23, no. 6, pp. 1204–1214, 2014.

[9] J.-H. Park, P. Stegall, and S. K. Agrawal, "Dynamic brace for correction of abnormal postures of the human spine," in *Proc. IEEE Int. Conf. Robot. Autom.*, May 2015, pp. 5922–5927.

[10] J. P. Merlet, *Parallel Robots* (Solid Mechanics and Its Applications), vol. 128. 2010, pp. 2091–2127.

[11] M. Luces, J. K. Mills, and B. Benhabib, "A review of redundant parallel kinematic mechanisms," *J. Intell. Robot. Syst.*, vol. 86, no. 2, pp. 175–198, 2017.

[12] Y. Lou, Y. Zhang, R. Huang, X. Chen, and Z. Li, "Optimization algorithms for kinematically optimal design of parallel manipulators," *IEEE Trans. Autom. Sci. Eng.*, vol. 11, no. 2, pp. 574–584, Apr. 2014.

[13] T. Nozaki, T. Mizoguchi, and K. Ohnishi, "Decoupling strategy for position and force control based on modal space disturbance observer," *IEEE Trans. Ind. Electron.*, vol. 61, no. 2, pp. 1022–1032, Feb. 2014.

[14] A. A. Allais, J. E. Mcinroy, and J. F. O'Brien, "Locally decoupled micromanipulation using an even number of parallel force actuators," *IEEE Trans. Robot.*, vol. 28, no. 6, pp. 1323–1334, Dec. 2012.

[15] C. Gosselin and S. Foucault, "Dynamic point-to-point trajectory planning of a two-DOF cable-suspended parallel robot," *IEEE Trans. Robot.*, vol. 30, no. 3, pp. 728–736, Jun. 2014.

[16] X. Jiang and C. Gosselin, "Dynamic point-to-point trajectory planning of a three-DOF cable-suspended parallel robot," *IEEE Trans. Robot.*, vol. 32, no. 6, pp. 1550–1557, Dec. 2016.

[17] J. Borrás, F. Thomas, and C. Torras, "New geometric approaches to the analysis and design of Stewart–Gough platforms," *IEEE/ASME Trans. Mechatronics*, vol. 19, no. 2, pp. 445–455, Apr. 2014.

[18] G. Mottola, C. Gosselin, and M. Carricato, "Dynamically-feasible elliptical trajectories for fully constrained 3-DOF cable-suspended parallel robots," in *Cable-Driven Parallel Robots*. 2018, pp. 219–230.

[19] J. Pile and N. Simaan, "Modeling, design, and evaluation of a parallel robot for cochlear implant surgery," *IEEE/ASME Trans. Mechatronics*, vol. 19, no. 6, pp. 1746–1755, Dec. 2014.

[20] P. K. Jamwal, S. Q. Xie, S. Hussain, and J. G. M. Parsons, "An adaptive wearable parallel robot for the treatment of ankle injuries," *IEEE/ASME Trans. Mechatronics*, vol. 19, no. 1, pp. 64–75, Feb. 2014.

[21] P. Dion-Gauvin and C. Gosselin, "Trajectory planning for the static to dynamic transition of point-mass cable-suspended parallel mechanisms," *Mech. Mach. Theory*, vol. 113, pp. 158–178, Jul. 2017.

[22] Y. Jiang, T. Li, L. Wang, and F. Chen, "Improving tracking accuracy of a novel 3-DOF redundant planar parallel kinematic machine," *Mech. Mach. Theory*, vol. 119, pp. 198–218, Jan. 2018.

[23] J. Wang, J. Wu, L. Wang, and Z. You, "Dynamic feed-forward control of a parallel kinematic machine," *Mechatronics*, vol. 19, no. 3, pp. 313–324, 2009.

[24] A. Dumlu and K. Erenturk, "Trajectory tracking control for a 3-DOF parallel manipulator using fractional-order $PI^{\lambda}D^{\mu}$ control," *IEEE Trans. Ind. Electron.*, vol. 61, no. 7, pp. 3417–3426, Jul. 2014.

[25] S.-H. Chen and L.-C. Fu, "Output feedback sliding mode control for a stewart platform with a nonlinear observer-based forward kinematics solution," *IEEE Trans. Control Syst. Technol.*, vol. 21, no. 1, pp. 176–185, Jan. 2012.

[26] S. Mishra, P. S. Londhe, S. Mohan, S. K. Vishvakarma, and B. M. Patre, "Robust task-space motion control of a mobile manipulator using a nonlinear control with an uncertainty estimator," *Comput. Elect. Eng.*, vol. 67, pp. 729–740, Apr. 2018.

[27] S. A. A. Moosavian and E. Papadopoulos, "Modified transpose Jacobian control of robotic systems," *Automatica*, vol. 43, no. 7, pp. 1226–1233, 2007.

[28] S.-H. Kim, Y. J. Shin, K.-S. Kim, and S. Kim, "Design and control of robot manipulator with a distributed actuation mechanism," *Mechatronics*, vol. 24, no. 8, pp. 1223–1230, 2014.

[29] Y. Pi and X. Wang, "Observer-based cascade control of a 6-DOF parallel hydraulic manipulator in joint space coordinate," *Mechatronics*, vol. 20, no. 6, pp. 648–655, 2010.

[30] S. H. Chen and L. C. Fu, "Observer-based backstepping control of a 6-DOF parallel hydraulic manipulator," *Control Eng. Pract.*, vol. 36, pp. 100–112, Mar. 2015.

[31] C. Yang, Z. Qu, and J. Han, "Decoupled-space control and experimental evaluation of spatial electrohydraulic robotic manipulators using singular value decomposition algorithms," *IEEE Trans. Ind. Electron.*, vol. 61, no. 7, pp. 3427–3438, Jul. 2014.

[32] C. Yang and J. Han, "Dynamic coupling analysis of a spatial 6-DOF electro-hydraulic parallel manipulator using a modal decoupling method," *Int. J. Adv. Robot. Syst.*, vol. 10, no. 2, p. 104, 2013.

[33] M. W. Spong and M. Vidyasagar, *Robot Dynamics and Control*, 2nd ed. Hoboken, NJ, USA: Wiley, 2008, pp. 193–229.

[34] A. G. Ruiz, J. C. Santos, J. Croes, W. Desmet, and M. M. da Silva, "On redundancy resolution and energy consumption of kinematically redundant planar parallel manipulators," *Robotica*, vol. 36, no. 6, pp. 809–821, 2018.

[35] L. J. Puglisi, R. Saltaren, C. Garcia, P. Cardenas, and H. Moreno, "Implementation of a generic constraint function to solve the direct kinematics of parallel manipulators using Newton–Raphson approach," *J. Control Eng. Appl. Inform.*, vol. 19, no. 2, pp. 71–79, 2017.
[36] S. Staicu, "Dynamics of the 6-6 Stewart parallel manipulator," *Robot. Comput.-Integr. Manuf.*, vol. 27, no. 1, pp. 212–220, 2011.
[37] C. Yang, J. Zhao, L. Li, and S. K. Agrawal, "Design and implementation of a novel modal space active force control concept for spatial multi-DOF parallel robotic manipulators actuated by electrical actuators," *ISA Trans.*, vol. 72, pp. 273–286, Jan. 2018.

XINJIAN NIU received the B.E. degree in mechatronics engineering from the Anhui University of Technology, Maanshan, China, in 2012, and the M.S. degree in mechatronics engineering from the Harbin Institute of Technology, Harbin, China, in 2014, where he is currently pursuing the Ph.D. degree. His research interests include electric-hydraulic servo control, scoliosis brace system, parallel manipulator control, modal space active force control, and PD control with DGC.

CHIFU YANG received the B.S., M.S., and Ph.D. degrees in mechatronics engineering from the Harbin Institute of Technology (HIT), Harbin, China, in 2005, 2007, and 2012, respectively. Since 2013, he has been a Visiting Scholar with the Robotics and Rehabilitation Laboratory, Columbia University, New York, NY, USA.

He is currently an Associate Professor with the Department of Mechatronics Engineering, HIT, Harbin, China. His current research interest includes parallel robots, assistant-rehabilitation robotics, exoskeleton robot, and hydraulic driven technology. He is a member of American Society of Mechanical Engineers. He is also a member of the Editorial Board of *Advances and Applications in Mechanical Engineering and Technology* and the *International Journal of Control Engineering and Technology*.

BOWEN TIAN received the B.S. degree in marketing and the Ph.D. degree in business administration from the Huazhong University of Science and Technology, Wuhan, China, in 2010 and 2015, respectively. Since 2013, she has been a Visiting Scholar with Indiana University Bloomington, Bloomington, IN, USA. She is currently a Lecturer with the Department of Economic and Trade, School of Businesses Administration, Zhongnan University of Economics and Law, Wuhan. Her current research interest includes innovation management and enterprise strategic management.

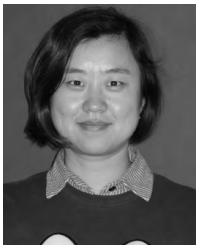

XIANG LI received the B.Eng. degree from the Department of Surveying and Mapping Engineering, Heilongjiang Institute of Technology, Harbin, China, in 2007. She is currently a Teaching Assistant with the Department of Engineering Graphics, School of Mechatronics Engineering, Harbin Institute of Technology, Harbin.

JUNWEI HAN received the Ph.D. degree in mechatronics engineering degree from the Harbin Institute of Technology, Harbin, China, in 1992. Since 1992, he has been a Researcher with China Earthquake Administration Institute of Engineering Mechanics. Since 1994, he has been a Researcher in mechanical engineering post-doctoral mobile stations with Harbin Industrial University. Since 1997, he has been a Professor with the Department of Mechatronics Engineering, Harbin Institute of Technology. He is currently the Academic Leader of fluid power transmission and control and the Director of the Institute of Simulation and Test of Electro-Hydraulic Servo System and the National State Key Laboratory of Robotics and System. He has authored or co-authored over 180 journal and conference articles. His main research interests include electro-hydraulic servo control, redundant-driven parallel control and flight simulation and simulation test system, six-degree-of-freedom (DOF) shaking table's vibration control, six-DOF motion simulation control system, and three-stage servo valve control technique with large flow and high response. He is a member of the Fluid Power Transmission and Control Association and a Council Member of the China Ordnance Society. He received the National Science and Technology Progress Award First Prize and Second Prize. He honored the Ministry of Education in the New Century Excellent Talents and the Defense Industry Young and Middle-Aged Expert with outstanding contributions.

SUNIL K. AGRAWAL (M'92) received the Ph.D. degree in mechanical engineering from Stanford University, Stanford, CA, USA, in 1990.

He is currently a Professor with the Department of Mechanical Engineering, Columbia University, New York, NY, USA. He has authored more than 300 journal and conference papers and two books in the areas of controlled mechanical systems, dynamic optimization, and robotics.

Dr. Agrawal is a fellow of the American Society of Mechanical Engineers (ASME). He received the Presidential Faculty Fellowship from the White House in 1994, the Bessel Prize in Germany in 2003, and the Humboldt U.S. Senior Scientist Award in 2007. He has been an editorial board member of several journals published by the ASME and the IEEE.